THE JOURNAL OF PHYSICAL CHEMISTRY LETTERS
A JOURNAL OF THE AMERICAN CHEMICAL SOCIETY

pubs.acs.org/JPCL

Letter

Size Dependence of Ultrafast Electron Transfer from Didodecyl Dimethylammonium Bromide-Modified $CsPbBr_3$ Nanocrystals to Electron Acceptors

Qiaoyun Wu, Lin Cheng, Pan Liang,* Rongrong Hu,* Bobo Yang, Jinlei Li, Yuanyuan Wang, Xiaoyang Li, Jun Zou, and Donghai Feng*

Cite This: *J. Phys. Chem. Lett.* 2024, 15, 7133−7140

Read Online

ACCESS | Metrics & More | Article Recommendations | Supporting Information

ABSTRACT: Charge transfer efficiencies in all-inorganic lead halide perovskite nanocrystals (NCs) are crucial for applications in photovoltaics and photocatalysis. Herein, $CsPbBr_3$ NCs with different sizes are synthesized by varying the ligand contents of didodecyl dimethylammonium bromide at room temperature. Adding benzoquinone (BQ) molecules leads to a decrease in the PL intensities and PL decay times in NCs. The electron transfer (ET) efficiency (η_{ET}) increases with NC size in complexes of $CsPbBr_3$ NCs and BQ molecules (NC-BQ complexes), when the same concentration of BQ is maintained, as investigated by transient photobleaching and photoluminescence spectroscopies. Controlling the same number of attached BQ acceptor molecules per NC induces the same η_{ET} in NC-BQ complexes even though with different NC sizes. Our findings provide new insights into ultrafast charge transfer behaviors in perovskite NCs, which is important for designing efficient light energy conversion devices.

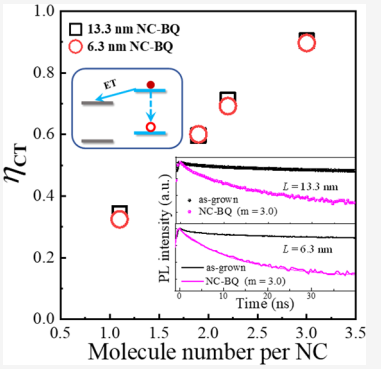

All-inorganic perovskite nanocrystals (NCs) exhibit excellent properties, including high photoluminescence quantum yields (PLQYs),[1] high carrier mobilities,[2] long carrier lifetimes,[3] and wide emission wavelength tunabilities over the entire visible range,[4] offering wide-ranging prospects for applications in light-emitting diodes,[5−7] lasers,[8] solar cells,[9] displays,[10] photodetectors,[11] and photocatalysis.[12−14] Most reported $CsPbX_3$ NCs are synthesized at high temperatures (>140 °C) in an inert environment according to a "hot-injection" method. The sizes of perovskite NCs can be controlled by adjusting the reaction temperatures during "hot injection"[15] or by altering the amounts of alkylammonium bromide salt.[16] However, the complex process of the "hot-injection" method has significantly limited its large-scale production. Compared with the "hot-injection" method, the room-temperature method under ambient air conditions is more convenient, feasible, and economically attractive. In addition, using the room-temperature method, the sizes of $CsPbBr_3$ NCs also can be precisely controlled[17] and the number of surface defects of $CsPbBr_3$ NCs can be reduced[18] by changing the ligands, which promotes their application in optoelectronic devices.[17−22]

The charge transfer (CT) times and efficiencies are important factors for high-performance photocatalysis and solar cells.[23−28] Donor−acceptor complexes are usually used to investigate the ultrafast CT processes.[25−27] Benzoquinone (BQ) molecules are well-known electron acceptors for perovskite NCs.[23,26,27] In the presence of BQ molecules, the photogenerated excitons of $CsPbBr_3$ NCs can be effectively separated, and the electron transfer (ET) and backward charge recombination (CR) found to be shortened, compared with those of as-grown NCs.[29] Very recently, it has been reported that adding BQ molecules in $CsPbBr_3$ NCs leads to a fast ET process and extraordinarily long-lived CS, which can up to a dozen days under ambient conditions, after light illumination.[23] It is generally known that the ET times decrease with an increase in BQ concentration.[26,29] Size-dependent effects could also play an important role in the CT processes. With a decrease in the sizes of $CsPbI_3$ NCs, the CT time decreases,[30] and similar phenomena have also been reported in conventional II−VI semiconductor NCs.[31] However, how the CT efficiencies change with NC sizes when controlling the same acceptor molecule number per NC is still an open question.

In this work, $CsPbBr_3$ NCs with various sizes are synthesized by adjusting the content of didodecyl dimethylammonium bromide (DDAB) as a ligand at room temperature under an air atmosphere. The transient dynamics are studied in colloidal $CsPbBr_3$ NCs with and without BQ molecules by using time-resolved photoluminescence (PL) and differential transmission measurements. After the addition of BQ electron acceptors, the

Received: May 25, 2024
Revised: June 28, 2024
Accepted: July 2, 2024
Published: July 3, 2024

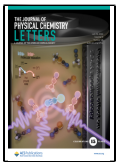

https://doi.org/10.1021/acs.jpclett.4c01543
J. Phys. Chem. Lett. 2024, 15, 7133−7140

Scheme 1. (a) Energy Level Diagram of BQ Molecules and $CsPbBr_3$ NCs with Weak and Strong Confinement[a] and (b) Schematic Structure of the Perovskite Lattice and BQ Molecules

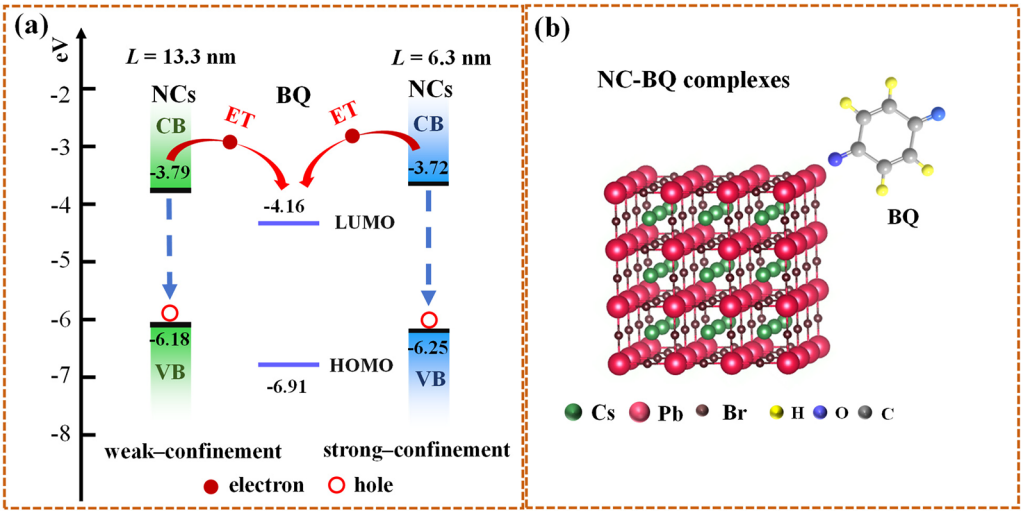

[a]The lowest electron (hole) energy levels in conduction (valence) bands of $CsPbBr_3$ NCs with sizes of 13.3 and 6.3 nm are indicated by black lines. The blue lines indicate the lowest unoccupied molecular orbital (LUMO) and highest occupied molecular orbital (HOMO) of BQ molecules. The ET from NCs to BQ and electron−hole radiative recombination processes are shown by red and dashed arrows, respectively.

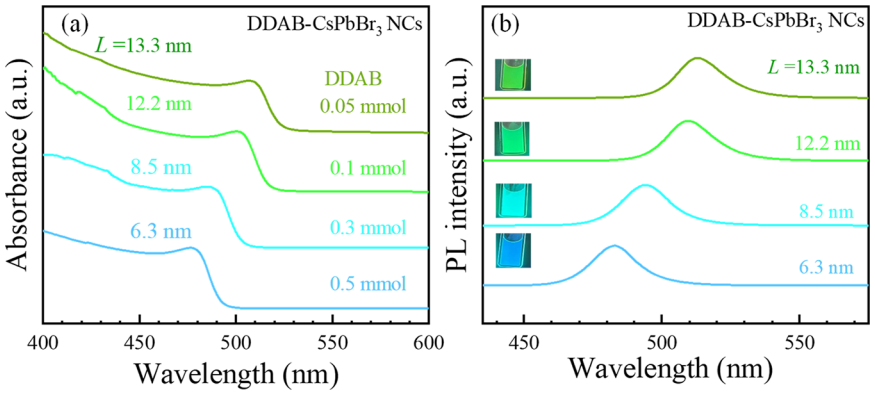

Figure 1. (a) Absorption and (b) PL spectra of $CsPbBr_3$ NCs with different NC sizes (edge length L as indicated). Plots are offset for the sake of clarity. The insets show photographs of didodecyl dimethylammonium bromide (DDAB)-modified $CsPbBr_3$ NCs under 365 nm irradiation.

PL intensities and PL decay times in NC-BQ complexes with different sizes of NCs decrease due to the ET processes as shown in Scheme 1. The ET efficiency (η_{ET}) increases with $CsPbBr_3$ NC size, when adding the same concentration of BQ molecules, because the number of attached BQ acceptor molecules per $CsPbBr_3$ NC (termed m below) is higher in NC-BQ complexes with a larger NC size. However, maintaining an equal value of m results in the same η_{ET} in all of the NC-BQ complexes with different NC sizes. These findings manifest that the transient interfacial η_{ET} in NC-BQ complexes is mainly dependent on the m values rather than the NC sizes.

$CsPbBr_3$ NCs with different concentrations of DDAB ligands were synthesized on the basis of the reported literature at room temperature under an air atmosphere.[17] Adding the DDAB ligands in amounts of 0.05, 0.1, 0.3, and 0.5 mmol can significantly affect the absorption and PL emission peaks of DDAB-modified $CsPbBr_3$ NCs. The first exciton absorption peaks of as-grown $CsPbBr_3$ NCs are blue-shifted from 509 to 477 nm with an increase in DDAB ligand concentration, and the corresponding PL emission peaks are blue-shifted from 512 to 480 nm, as shown in panels a and b, respectively, of Figure 1. In comparison, an only ∼6 nm PL peak shift happened upon addition of different contents of conventional OAm ligands (see Figure S1). It is known that the shifted emission peak is correlated with the NC size and bandgap of $CsPbBr_3$ NCs,[15,32] indicating that DDAB ligands have better size control for $CsPbBr_3$ NCs compared to conventional OAm ligands when using room-temperature methods. The detailed synthesis procedures can be found in the experimental section in the Supporting Information.

The representative transmission electron microscopy (TEM) images of as-grown $CsPbBr_3$ NCs with different concentrations of DDAB exhibit typical orthogonal shapes (see Figure S2a,b) and consistent with previous reports.[17] The lattice sizes of $CsPbBr_3$ with the addition of 0.05 and 0.5 mmol of DDAB ligands are 0.37 and 0.29 nm, respectively, corresponding to the (110) and (220) phases of $CsPbBr_3$, respectively. According to TEM images, the sizes of $CsPbBr_3$ NCs with addition of 0.05 and 0.5 mmol of DDAB ligands are 13.3 and 6.3 nm, respectively. Considering the relationship between the absorption peak position and the bulk band edge,[33] for the NCs with a large size of 13.3 nm, the potentials of the lowest electron and hole energy levels are −3.79 and −6.18 eV (relative to vacuum), respectively,[29] while for the

https://doi.org/10.1021/acs.jpclett.4c01543
J. Phys. Chem. Lett. 2024, 15, 7133−7140

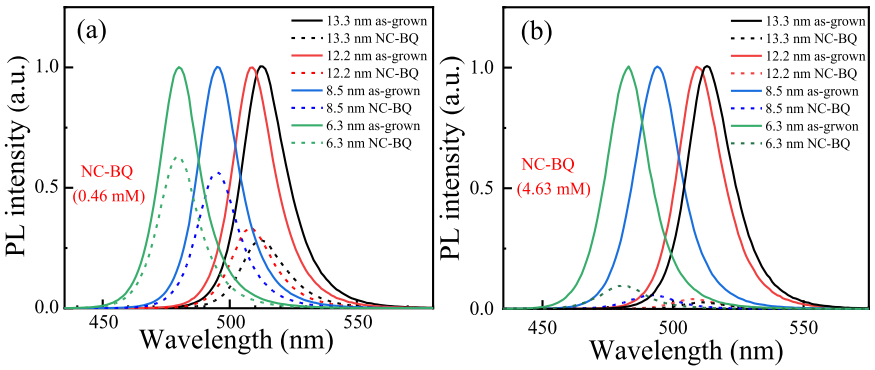

Figure 2. PL spectra of as-grown $CsPbBr_3$ NCs (normalized solid lines) and NC-BQ complexes (dashed lines) for different BQ concentration of (a) 0.46 mM and (b) 4.63 mM (b).

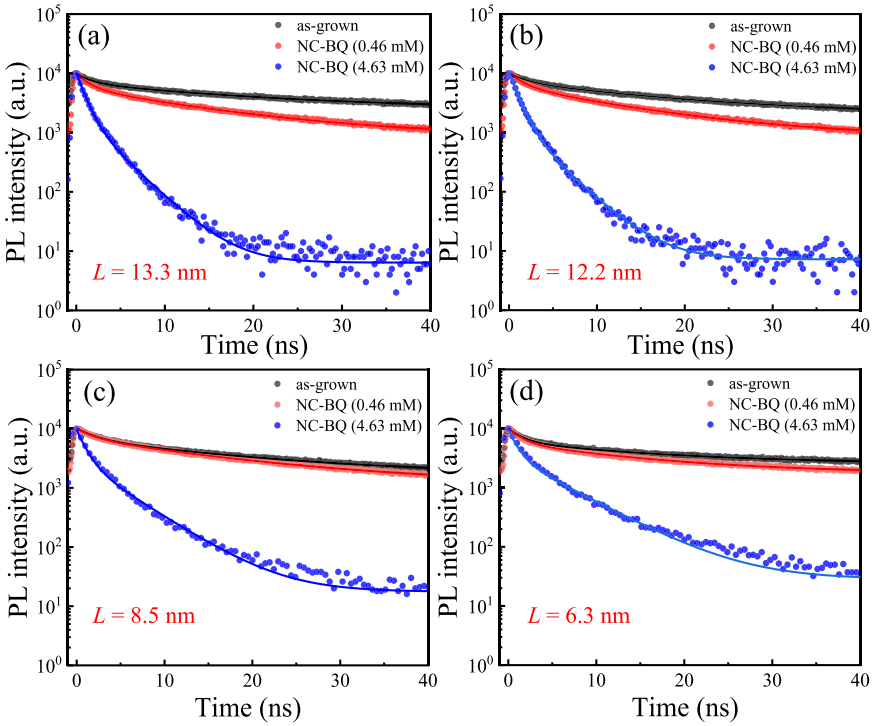

Figure 3. PL decay curves of as-grown $CsPbBr_3$ NCs and NC-BQ complexes with different sizes of NCs. The BQ concentrations are 0.46 and 4.63 mM in the NC-BQ complexes. The initial PL intensities are normalized to the same values.

NCs with a small size of 6.3 nm, the potentials of the lowest electron and hole energy levels are −3.72 and −6.25 eV, respectively (detailed calculation information can be found in the Supporting Information). The bandgap energy (E_g) and the corresponding NC size can be calculated through their absorption spectra.[4,34] As shown in Figure S3, the E_g values of $CsPbBr_3$ NCs with 0.05, 0.1, 0.3, and 0.5 mmol of DDAB ligands are calculated, and thus, the sizes of $CsPbBr_3$ NCs of 13.3, 12.2, 8.5, and 6.3 nm, respectively, can be obtained. The calculated sizes of the largest and smallest NCs are in line with the TEM results in Figure S2. Therefore, increasing the concentrations of the DDAB ligand, along with the blue-shifted wavelengths in PL peaks and first absorption peaks of NCs, results in an increase in E_g and a decrease in NC size.

The first exciton absorption peaks of as-grown $CsPbBr_3$ NCs and their corresponding NC-BQ complexes are almost the same (Figure S4), which is consistent with previous reports.[23,29] Panels a and b of Figure 2 show the PL spectra of as-grown NCs with different NC sizes and their corresponding NC-BQ complexes. Compared with as-grown NCs, the addition of BQ molecules can effectively quench their PL intensities. At the same BQ concentration, the quenching efficiencies increase with NC size. As shown in Figure 2a, at a BQ concentration of 0.46 mM, the PL quenching efficiencies are 72% for the largest size (L = 13.3 nm) and 37% for the smallest size (L = 6.3 nm). With an increase in the concentration of BQ molecules to 4.63 mM, the PL intensities of 13.3 nm $CsPbBr_3$ NCs can be almost completely quenched, while the PL intensity decreased to ∼10% of that in 6.3 nm $CsPbBr_3$ NCs. The photogenerated electrons in the conduction band of $CsPbBr_3$ NCs can be rapidly captured by the BQ molecules within a few tens of picoseconds,[29] leading to a PL quenching of $CsPbBr_3$ NCs, and increasing the concentration of BQ molecules accelerates the ET processes.

Time-correlated single-photon counting (TCSPC) was employed to investigate the time-resolved PL of as-grown $CsPbBr_3$ NCs and NC-BQ complexes. As shown in Figure 3, all of the PL decay curves of as-grown $CsPbBr_3$ NCs and

https://doi.org/10.1021/acs.jpclett.4c01543
J. Phys. Chem. Lett. 2024, 15, 7133−7140

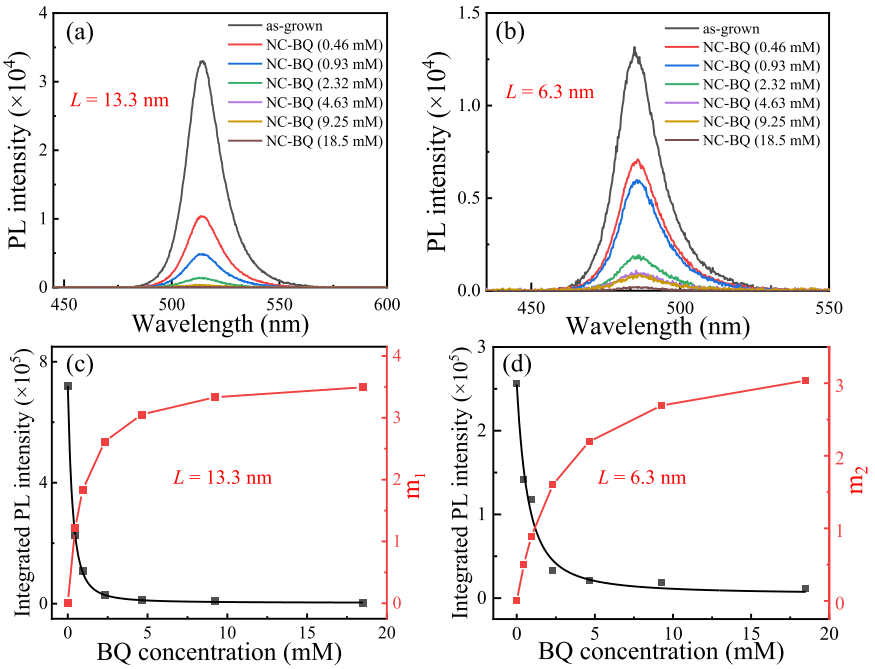

Figure 4. BQ concentration-dependent PL intensity for $CsPbBr_3$ NC sizes of (a) 13.3 nm and (b) 6.3 nm. Integrated PL intensities (black lines) and the *m* values (red lines) as a function of BQ concentrations for $CsPbBr_3$ NC sizes of (c) 13.3 nm and (d) 6.3 nm.

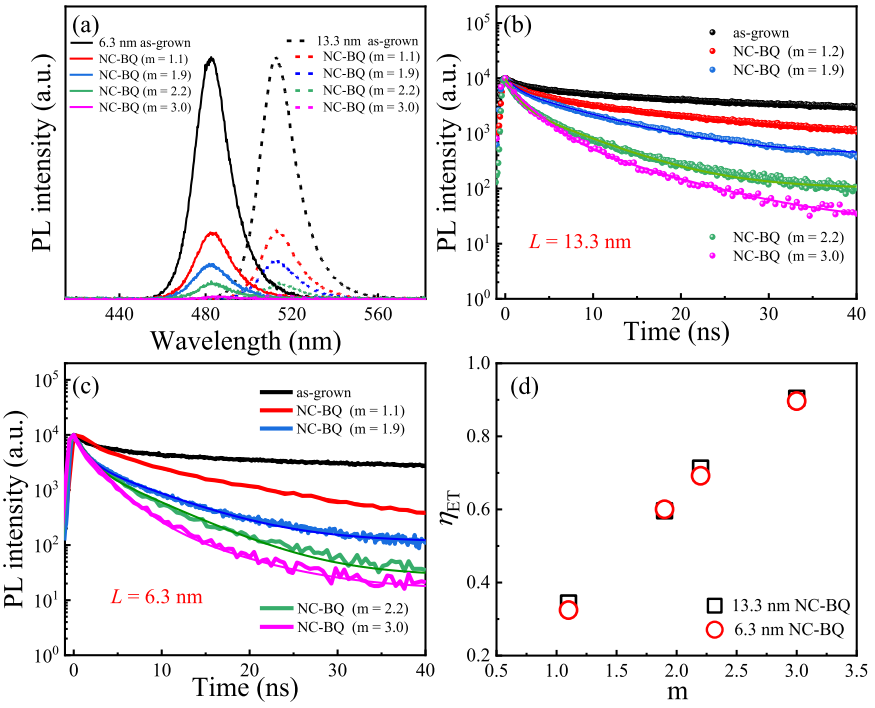

Figure 5. (a) PL spectra of as-grown $CsPbBr_3$ NCs with NCs sizes of 6.3 and 13.3 nm and the corresponding NC-BQ complexes with different *m* values. Time-resolved PL spectra of as-grown $CsPbBr_3$ NCs and NC-BQ complexes with different *m* values with NC sizes of (b) 13.3 nm and (c) 6.3 nm. (d) η_{ET} as a function of *m* value.

corresponding NC-BQ complexes can be fitted well by a biexponential decay function. Detailed PL decay times and the corresponding amplitudes are listed in Table S1. According to the previous reports, the fast (τ_1) and slow (τ_2) decay components can be attributed to nonradiative recombination and radiative recombination, respectively.[35−38] The fitted fast and slow decay lifetimes for as-grown $CsPbBr_3$ NCs decrease from 2.01 to 1.70 ns and from 21.0 to 16.1 ns, respectively, when the size of the NCs was reduced from 13.3 to 6.3 nm, and the average lifetimes (as defined in the Supporting Information) of as-grown $CsPbBr_3$ NCs decrease from 19.8 to 14.5 ns with a decrease in NC size. Compared to as-grown $CsPbBr_3$ NCs, NC-BQ complexes show smaller τ_1 and τ_2 values due to the ET processes from the $CsPbBr_3$ NCs to BQ molecules. For 13.3 nm NCs and 4.63 mM BQ, τ_1 and τ_2 are significantly reduced to 0.92 and 3.1 ns, respectively. With a

https://doi.org/10.1021/acs.jpclett.4c01543
J. Phys. Chem. Lett. 2024, 15, 7133−7140

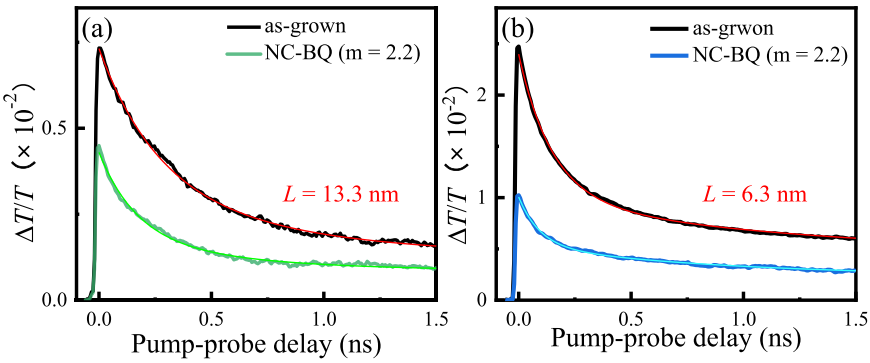

Figure 6. Time-resolved differential transmission spectra of as-grown $CsPbBr_3$ and NC-BQ complexes for NC sizes of (a) 13.3 nm and (b) 6.3 nm. The wavelengths of the probe and pump pulses are at their corresponding first excitation absorption peaks.

decrease in NC size from 13.3 to 6.3 nm, fast decay component τ_1 and slow decay component τ_2 increase from 0.92 to 1.24 ns and from 3.1 to 6.0 ns, respectively, when adding BQ molecules at a concentration of 4.63 mM, which show a trend that is the opposite of that in as-grown NCs. Similar experimental phenomena are also observed in transient photobleaching measurements (see Figure S5). We calculated the η_{ET} for these samples by using eq S5. The η_{ET} of the 13.3 nm NC-BQ complexes is 90%, much larger than that of the 6.3 nm sample ($\eta_{ET} \sim 70\%$), when adding the same concentration of BQ molecules (~4.63 mM). A similar trend was also observed when the BQ concentration decreased to 0.46 mM, suggesting that η_{ET} increased with NC size in the NC-BQ complexes when keeping the same BQ concentration, which is consistent with the PL quenching phenomena as shown in Figure 2.

To further demonstrate the interfacial ET mechanism, the relationship between BQ concentrations and PL intensities of $CsPbBr_3$ NCs with different sizes is investigated. The PL spectra of 13.3 and 6.3 nm as-grown $CsPbBr_3$ NCs and their corresponding NC-BQ complexes with different concentrations of BQ are shown in panels a and b of Figure 4. For 13.3 and 6.3 nm NCs, increasing the BQ concentration decreases the PL intensity. The adsorption of BQ molecules onto NCs surfaces is governed by the Langmuir adsorption isotherm and follows a Poissonian distribution.[39] The integrated PL intensities and determination of m values for 13.3 and 6.3 nm NCs as a function of BQ concentrations are plotted in panels c and d of Figure 4 (detailed calculation information can be found in the Supporting Information). As shown in panels c and d of Figure 4, with an increase in the BQ concentration (thus the m value), the integrated PL intensities decrease for both large and small NC-BQ complexes. Note that, when the NC size is decreased along with an increased E_g, the driving force increases in NC-BQ complexes, which accelerates the ET process. However, at the same BQ concentrations, the m value is smaller in 6.3 nm NCs than in 13.3 nm NCs, which plays the dominant role in the ET processes, resulting in longer ET times and thus longer decay times in 6.3 nm NCs as shown in Figure 3.

To further investigate how η_{ET} changes with NC size, comparative steady state PL and time-resolved PL measurements in as-grown $CsPbBr_3$ NCs with sizes of 13.3 and 6.3 nm and their corresponding NC-BQ complexes with the same m values are carried out. As shown in Figure 5a, one can see that the degrees of PL quenching remain the same for both sizes of NCs, when controlling the same m values. Panels b and c of Figure 5 show the PL decays of as-grown $CsPbBr_3$ NCs with different sizes of 6.3 and 13.3 nm and their corresponding NC-BQ complexes with different m values. The PL decay times are listed in Table S2. As shown in Figure 5b, as-grown $CsPbBr_3$ NCs with a size of 13.3 nm exhibit an average PL decay lifetime of ~19.8 ns, while adding a BQ electron acceptor with a concentration of 1.42 mM (equal to $m_1 = 2.2$) reduces the average PL lifetime to 5.7 ns, showing η_{ET} is 71%. Similarly, as shown in Figure 5c, the average PL lifetime of as-grown $CsPbBr_3$ NCs with a size of 6.3 nm is 14.5 ns. Upon addition of BQ molecules at a concentration of 4.63 mM (also equal to $m_2 = 2.2$), the PL lifetime decreases to 4.4 ns, showing an η_{ET} of 70%. With a change in the m values, NC-BQ complexes with different sizes exhibited almost the same η_{ET}. Figure 5d shows η_{ET} as a function of the m values in NCs with both sizes. η_{ET} increases with an increase in the m value in both sizes of NCs. In addition, the η_{ET} values remain the same in NCs with different sizes when keeping the same m values. This phenomenon further reveals that, despite the varying sizes of NCs, regulating the same m value results in the same degrees of PL quenching and the same η_{ET} values.

Further investigations of ultrafast charge dynamics in different-sized NCs with and without BQ but with the same m value are measured by using transient photobleaching spectra (or time-resolved differential transmission measurements).[40] The wavelengths of pump and probe pulses are set at the first exciton transition for each sample of $CsPbBr_3$ NCs and NC-BQ complexes. For as-grown $CsPbBr_3$ NCs with sizes of 13.3 and 6.3 nm, a pump fluence (F_p) of 20 $\mu J/cm^2$ produces an average of 0.74 and 0.038 electron–hole pair per NC (termed $\langle N \rangle$ below), respectively[41] (detailed calculation information can be found in the Supporting Information). Figure 6 shows the transient photobleaching dynamics of as-grown $CsPbBr_3$ NCs with sizes of 13.3 and 6.3 nm and their corresponding NC-BQ complexes with the same m value. All of the transient photobleaching dynamics exhibit two decay components, fast and slow decay (τ_{TA1} and τ_{TA2}, respectively). Figure 6a shows the transient photobleaching dynamics of as-grown NCs with an L of 13.3 nm, showing the fast and slow decay processes with a τ_{TA1} of 300 ps and a τ_{TA2} of 1130 ps. The fast decay component can be ascribed to the electron and/or hole trapping processes, while the slow decay component in photobleaching measurement is in accordance with the detected fast PL decay component and can be attributed to the nonradiative recombination processes.[29] The photobleaching dynamic in 13.3 nm NC-BQ complexes also shows a fast decay component τ_{TA1} of 185 ps and a slow decay component

https://doi.org/10.1021/acs.jpclett.4c01543
J. Phys. Chem. Lett. 2024, 15, 7133−7140

τ_{TA2} of 1000 ps. The shortening of τ_{TA1} and τ_{TA2} after adding BQ molecules, compared with that of in as-grown NCs, can be attributed to ET from the conduction bands of $CsPbBr_3$ NCs to LUMO of BQ electron acceptors. The transfer efficiencies of the fast and slow processes are 38% and 12%, respectively. As shown in Figure 6b, as-grown $CsPbBr_3$ NCs and NC-BQ complexes with a size of 6.3 nm exhibit similar phenomena but with different decay time constants, compared with that in 13.3 nm NCs. The times of fast and slow decay processes are as follows: τ_{TA1} = 120 ps and τ_{TA2} = 800 ps in 6.3 nm as-grown NCs, which is faster than that in 13.3 nm NCs. For the 6.3 nm NC-BQ complexes, the lifetimes of fast and slow decay components change to a τ_{TA1} of 71 ps and a τ_{TA2} of 700 ps. The two processes show transfer efficiencies of 41% and 13%, respectively. The detailed parameters are listed in Table S3. Note that the ratios of time constants between NCs with and without BQ are nearly independent of pump fluence (or $\langle N \rangle$), as shown in Figure S6 and Table S4. According to the results presented above, we can conclude that controlling the same m value can obtain the same ET efficiencies in NC-BQ complexes even with different sizes.

In conclusion, $CsPbBr_3$ NCs with various sizes have been synthesized by varying the contents of the DDAB ligand at room temperature under an air atmosphere. Electron acceptor BQ molecules are employed to investigate the ultrafast interfacial ET processes from $CsPbBr_3$ NCs by using time-resolved PL and differential transmission spectra. The addition of BQ molecules can effectively quench the PL in all-sized $CsPbBr_3$ NCs. Upon addition of the same concentration of BQ molecules, η_{ET} increases with NC size, due to the fact that the number of BQ molecules per NC is larger in larger NCs. When the same number of BQ molecules per NC is maintained, both the degree of PL quenching and η_{ET} in NC-BQ complexes are almost the same for different NC sizes. This reveals that the acceptor number per NC is the dominant factor for controlling the efficiency of interfacial ET processes, as compared with NC sizes.

■ ASSOCIATED CONTENT

Supporting Information

The Supporting Information is available free of charge at https://pubs.acs.org/doi/10.1021/acs.jpclett.4c01543.

Sample preparation, optical and spectroscopic measurements, energetic estimations for $CsPbBr_3$ NCs, PL spectra of $CsPbBr_3$ NCs with different types of ligands, TEM images of DDAB-capped $CsPbBr_3$ NCs, determination of the bandgap energy levels of DDAB-capped $CsPbBr_3$ NCs, absorption spectra of as-grown $CsPbBr_3$ NCs and NC-BQ complexes, kinetic fitting of PL decays in as-grown $CsPbBr_3$ NCs and NC-BQ complexes, calculation of electron transfer efficiencies, number of BQ acceptor molecules attached per NC, calculation of the number of excited electron−hole pairs per NC, kinetic fitting of transient photobleaching in as-grown $CsPbBr_3$ NCs and NC-BQ complexes, and pump fluence dependence of transient photobleaching signals (PDF)

■ AUTHOR INFORMATION

Corresponding Authors

Rongrong Hu − *School of Science, Shanghai Institute of Technology, Shanghai 201418, China;* orcid.org/0009-0004-0803-9599; Email: hrr92@sit.edu.cn

Pan Liang − *College of Arts and Sciences, Shanghai Dianji University, Shanghai 201306, China*; Email: liangp@sdju.edu.cn

Donghai Feng − *State Key Laboratory of Precision Spectroscopy, East China Normal University, Shanghai 200241, China; Collaborative Innovation Center of Extreme Optics, Shanxi University, Taiyuan, Shanxi 030006, China;* orcid.org/0000-0003-3272-6482; Email: dhfeng@phy.ecnu.edu.cn

Authors

Qiaoyun Wu − *School of Science, Shanghai Institute of Technology, Shanghai 201418, China*

Lin Cheng − *State Key Laboratory of Precision Spectroscopy, East China Normal University, Shanghai 200241, China*

Bobo Yang − *School of Science, Shanghai Institute of Technology, Shanghai 201418, China;* orcid.org/0000-0003-1351-947X

Jinlei Li − *State Key Laboratory of Precision Spectroscopy, East China Normal University, Shanghai 200241, China;* orcid.org/0000-0001-8211-8392

Yuanyuan Wang − *School of Science, Shanghai Institute of Technology, Shanghai 201418, China*

Xiaoyang Li − *School of Science, Shanghai Institute of Technology, Shanghai 201418, China*

Jun Zou − *School of Science, Shanghai Institute of Technology, Shanghai 201418, China;* orcid.org/0000-0003-4720-2040

Complete contact information is available at: https://pubs.acs.org/10.1021/acs.jpclett.4c01543

Notes

The authors declare no competing financial interest.

■ ACKNOWLEDGMENTS

This work is supported by the National Natural Science Foundation of China (Grants 12104311, 12174108, and 12004239), the Shanghai Chenguang Program (Grant 22CGA74), the National Key R&D Program of China (Grant 2021YFB3501700), the Shanghai Science and Technology Committee (STCSM) Science and Technology Innovation Program (Grants 22N21900400 and 23N21900100), the Key R&D Program of Jiangsu Province (Grant BE2023048), and the Key R&D Program of Zhejiang Province (Grant 2024C01193).

■ REFERENCES

(1) Gong, X.; Voznyy, O.; Jain, A.; Liu, W.; Sabatini, R.; Piontkowski, Z.; Walters, G.; Bappi, G.; Nokhrin, S.; Bushuyev, O.; Yuan, M.; Comin, R.; McCamant, D.; Kelley, S. O.; Sargent, E. H. Electron−Phonon Interaction in Efficient Perovskite Blue Emitters. *Nat. Mater.* **2018**, *17*, 550−556.

(2) Lim, J.; Kober-Czerny, M.; Lin, Y.-H.; Ball, J. M.; Sakai, N.; Duijnstee, E. A.; Hong, M. J.; Labram, J. G.; Wenger, B.; Snaith, H. J. Long-Range Charge Carrier Mobility in Metal Halide Perovskite Thin-Films and Single Crystals via Transient Photo-Conductivity. *Nat. Commun.* **2022**, *13*, 4201.

(3) De Quilettes, D. W.; Vorpahl, S. M.; Stranks, S. D.; Nagaoka, H.; Eperon, G. E.; Ziffer, M. E.; Snaith, H. J.; Ginger, D. S. Impact of Microstructure on Local Carrier Lifetime in Perovskite Solar Cells. *Science* **2015**, *348*, 683−686.

(4) Protesescu, L.; Yakunin, S.; Bodnarchuk, M. I.; Krieg, F.; Caputo, R.; Hendon, C. H.; Yang, R. X.; Walsh, A.; Kovalenko, M. V. Nanocrystals of Cesium Lead Halide Perovskites ($CsPbX_3$, X = Cl, Br,

and I): Novel Optoelectronic Materials Showing Bright Emission with Wide Color Gamut. *Nano Lett.* **2015**, *15*, 3692−3696.
(5) Fakharuddin, A.; Gangishetty, M. K.; Abdi-Jalebi, M.; Chin, S.-H.; bin Mohd Yusoff, Abd. R.; Congreve, D. N.; Tress, W.; Deschler, F.; Vasilopoulou, M.; Bolink, H. J. Perovskite Light-Emitting Diodes. *Nat. Electron.* **2022**, *5*, 203−216.
(6) Li, J.; Ren, C.; Qiu, X.; Lin, X.; Chen, R.; Yin, C.; He, T. Ultrafast Optical Nonlinearity of Blue-Emitting Perovskite Nanocrystals. *Photon. Res.* **2018**, *6*, 554−559.
(7) Hu, R.; Peng, W.; Cheng, L.; Wu, Q.; Dong, G.; Liang, P.; Yang, B.; Li, Y.; Zou, J.; Feng, D. Enhancement of Photoluminescence in $CsPbBr_3$ Nanocrystals with 1-Octanethiol by Light Illumination for Potential Emitting Applications. *ACS Appl. Nano Mater.* **2024**, *7*, 12903−12910.
(8) Zhang, Q.; Shang, Q.; Su, R.; Do, T. T. H.; Xiong, Q. Halide Perovskite Semiconductor Lasers: Materials, Cavity Design, and Low Threshold. *Nano Lett.* **2021**, *21*, 1903−1914.
(9) Yoo, J. J.; Seo, G.; Chua, M. R.; Park, T. G.; Lu, Y.; Rotermund, F.; Kim, Y.-K.; Moon, C. S.; Jeon, N. J.; Correa-Baena, J.-P.; Bulović, V.; Shin, S. S.; Bawendi, M. G.; Seo, J. Efficient Perovskite Solar Cells via Improved Carrier Management. *Nature* **2021**, *590*, 587−593.
(10) Wu, X.; Ji, H.; Yan, X.; Zhong, H. Industry Outlook of Perovskite Quantum Dots for Display Applications. *Nat. Nanotechnol.* **2022**, *17*, 813−816.
(11) Yang, T.; Zheng, Y.; Du, Z.; Liu, W.; Yang, Z.; Gao, F.; Wang, L.; Chou, K.; Hou, X.; Yang, W. Superior Photodetectors Based on All-Inorganic Perovskite $CsPbI_3$ Nanorods with Ultrafast Response and High Stability. *ACS Nano* **2018**, *12*, 1611−1617.
(12) Kong, Z.-C.; Liao, J.-F.; Dong, Y.-J.; Xu, Y.-F.; Chen, H.-Y.; Kuang, D.-B.; Su, C.-Y. Core@Shell $CsPbBr_3$@Zeolitic Imidazolate Framework Nanocomposite for Efficient Photocatalytic CO_2 Reduction. *ACS Energy Lett.* **2018**, *3*, 2656−2662.
(13) Li, N.; Chen, X.; Wang, J.; Liang, X.; Ma, L.; Jing, X.; Chen, D.-L.; Li, Z. ZnSe Nanorods−$CsSnCl_3$ Perovskite Heterojunction Composite for Photocatalytic CO_2 Reduction. *ACS Nano* **2022**, *16*, 3332−3340.
(14) Wu, X.; Xu, R.; Li, X.; Zeng, R.; Luo, B. Amino Acid-Assisted Preparation of Homogeneous PbS/$CsPbBr_3$ Nanocomposites for Enhanced Photoelectrocatalytic CO_2 Reduction. *J. Phys. Chem. C* **2022**, *126*, 15744−15751.
(15) Xu, F.; Kong, X.; Wang, W.; Juan, F.; Wang, M.; Wei, H.; Li, J.; Cao, B. Quantum Size Effect and Surface Defect Passivation in Size-Controlled $CsPbBr_3$ Quantum Dots. *J. Alloys Compd.* **2020**, *831*, 154834.
(16) Dutta, A.; Dutta, S. K.; Das Adhikari, S.; Pradhan, N. Tuning the Size of $CsPbBr_3$ Nanocrystals: All at One Constant Temperature. *ACS Energy Lett.* **2018**, *3*, 329−334.
(17) Chen, Z.; Mei, S.; He, H.; Wen, Z.; Cui, Z.; Yang, B.; Yang, D.; Zhang, W.; Xie, F.; Zou, J.; Guo, R. Rapid Large-Scale Synthesis of Highly Emissive Solid-State Metal Halide Perovskite Quantum Dots across the Full Visible Spectrum. *Opt. Laser Technol.* **2021**, *143*, 107369.
(18) Ye, F.; Zhang, H.; Li, W.; Yan, Y.; Cai, J.; Gurney, R. S.; Pearson, A. J.; Liu, D.; Wang, T. Ligand-Exchange of Low-Temperature Synthesized $CsPbBr_3$ Perovskite toward High-Efficiency Light-Emitting Diodes. *Small Methods* **2019**, *3*, 1800489.
(19) Veldhuis, S. A.; Ng, Y. F.; Ahmad, R.; Bruno, A.; Jamaludin, N. F.; Damodaran, B.; Mathews, N.; Mhaisalkar, S. G. Crown Ethers Enable Room-Temperature Synthesis of $CsPbBr_3$ Quantum Dots for Light-Emitting Diodes. *ACS Energy Lett.* **2018**, *3*, 526−531.
(20) Mo, Q.; Shi, T.; Cai, W.; Zhao, S.; Yan, D.; Du, J.; Zang, Z. Room Temperature Synthesis of Stable Silica-Coated $CsPbBr_3$ Quantum Dots for Amplified Spontaneous Emission. *Photon. Res.* **2020**, *8*, 1605−1612.
(21) Pan, J.; Quan, L. N.; Zhao, Y.; Peng, W.; Murali, B.; Sarmah, S. P.; Yuan, M.; Sinatra, L.; Alyami, N. M.; Liu, J.; Yassitepe, E.; Yang, Z.; Voznyy, O.; Comin, R.; Hedhili, M. N.; Mohammed, O. F.; Lu, Z. H.; Kim, D. H.; Sargent, E. H.; Bakr, O. M. Highly Efficient Perovskite-Quantum-Dot Light-Emitting Diodes by Surface Engineering. *Adv. Mater.* **2016**, *28*, 8718−8725.
(22) Jathar, S. B.; Rondiya, S. R.; Bade, B. R.; Nasane, M. P.; Barma, S. V.; Jadhav, Y. A.; Rokade, A. V.; Kore, K. B.; Nilegave, D. S.; Tandale, P. U.; Jadkar, S. R.; Funde, A. M. Facile Method for Synthesis of $CsPbBr_3$ Perovskite at Room Temperature for Solar Cell Applications. *ES Mater. Manuf.* **2021**, *12*, 72−77.
(23) Cheng, L.; Hu, R.; Jiang, M.; Men, Y.; Wang, Y.; Li, J.; Jia, T.; Sun, Z.; Feng, D. Extremely Long-Lived Charge Separation and Related Carrier Spin Excitation in $CsPbBr_3$ Perovskite Quantum Dots with an Electron Acceptor Benzoquinone. *Nano Res.* **2024**, DOI: 10.1007/s12274-024-6466-z.
(24) Kobosko, S. M.; DuBose, J. T.; Kamat, P. V. Perovskite Photocatalysis. Methyl Viologen Induces Unusually Long-Lived Charge Carrier Separation in $CsPbBr_3$ Nanocrystals. *ACS Energy Lett.* **2020**, *5*, 221−223.
(25) Venkateswarlu, D.; Swetha, T.; Akhil, S.; Palabathuni, M.; Mishra, N.; Singh, S. P. Surface Engineering of $CsPbBr_3$ Perovskite Nanocrystals: Hole Transfer Dynamics and Enhanced Photocurrent Response Using a Novel Organic Molecule. *Mater. Adv.* **2023**, *4*, 1935−1940.
(26) Li, Q.; Lian, T. Ultrafast Charge Separation in Two-Dimensional $CsPbBr_3$ Perovskite Nanoplatelets. *J. Phys. Chem. Lett.* **2019**, *10*, 566−573.
(27) Sarkar, S.; Ravi, V. K.; Banerjee, S.; Yettapu, G. R.; Markad, G. B.; Nag, A.; Mandal, P. Terahertz Spectroscopic Probe of Hot Electron and Hole Transfer from Colloidal $CsPbBr_3$ Perovskite Nanocrystals. *Nano Lett.* **2017**, *17*, 5402−5407.
(28) Zhang, P.; Zhu, G.; Shi, Y.; Wang, Y.; Zhang, J.; Du, L.; Ding, D. Ultrafast Interfacial Charge Transfer of Cesium Lead Halide Perovskite Films $CsPbX_3$ (X = Cl, Br, I) with Different Halogen Mixing. *J. Phys. Chem. C* **2018**, *122*, 27148−27155.
(29) Wu, K.; Liang, G.; Shang, Q.; Ren, Y.; Kong, D.; Lian, T. Ultrafast Interfacial Electron and Hole Transfer from $CsPbBr_3$ Perovskite Quantum Dots. *J. Am. Chem. Soc.* **2015**, *137*, 12792−12795.
(30) Shang, Q.; Kaledin, A. L.; Li, Q.; Lian, T. Size Dependent Charge Separation and Recombination in $CsPbI_3$ Perovskite Quantum Dots. *J. Chem. Phys.* **2019**, *151*, 074705.
(31) Zhu, H.; Yang, Y.; Hyeon-Deuk, K.; Califano, M.; Song, N.; Wang, Y.; Zhang, W.; Prezhdo, O. V.; Lian, T. Auger-Assisted Electron Transfer from Photoexcited Semiconductor Quantum Dots. *Nano Lett.* **2014**, *14*, 1263−1269.
(32) Luo, X.; Lai, R.; Li, Y.; Han, Y.; Liang, G.; Liu, X.; Ding, T.; Wang, J.; Wu, K. Triplet Energy Transfer from $CsPbBr_3$ Nanocrystals Enabled by Quantum Confinement. *J. Am. Chem. Soc.* **2019**, *141*, 4186−4190.
(33) Butler, K. T.; Frost, J. M.; Walsh, A. Band Alignment of the Hybrid Halide Perovskites $CH_3NH_3PbCl_3$, $CH_3NH_3PbBr_3$ and $CH_3NH_3PbI_3$. *Mater. Horiz.* **2015**, *2*, 228−231.
(34) Maes, J.; Balcaen, L.; Drijvers, E.; Zhao, Q.; De Roo, J.; Vantomme, A.; Vanhaecke, F.; Geiregat, P.; Hens, Z. Light Absorption Coefficient of $CsPbBr_3$ Perovskite Nanocrystals. *J. Phys. Chem. Lett.* **2018**, *9*, 3093−3097.
(35) Peng, W.; Hu, R.; Yang, B.; Wu, Q.; Liang, P.; Cheng, L.; Cheng, X.; Li, Y.; Zou, J. Solution-Grown Millimeter-Scale Mn-Doped $CsPbBr_3/Cs_4PbBr_6$ Crystals with Enhanced Photoluminescence and Stability for Light-Emitting Applications. *Phys. Chem. Chem. Phys.* **2024**, *26*, 373−380.
(36) Koscher, B. A.; Swabeck, J. K.; Bronstein, N. D.; Alivisatos, A. P. Essentially Trap-Free $CsPbBr_3$ Colloidal Nanocrystals by Postsynthetic Thiocyanate Surface Treatment. *J. Am. Chem. Soc.* **2017**, *139*, 6566−6569.
(37) Yettapu, G. R.; Talukdar, D.; Sarkar, S.; Swarnkar, A.; Nag, A.; Ghosh, P.; Mandal, P. Terahertz Conductivity within Colloidal $CsPbBr_3$ Perovskite Nanocrystals: Remarkably High Carrier Mobilities and Large Diffusion Lengths. *Nano Lett.* **2016**, *16*, 4838−4848.
(38) Makarov, N. S.; Guo, S.; Isaienko, O.; Liu, W.; Robel, I.; Klimov, V. I. Spectral and Dynamical Properties of Single Excitons,

https://doi.org/10.1021/acs.jpclett.4c01543
J. Phys. Chem. Lett. 2024, 15, 7133−7140

Biexcitons, and Trions in Cesium−Lead-Halide Perovskite Quantum Dots. *Nano Lett.* **2016**, *16*, 2349−2362.
(39) Morris-Cohen, A. J.; Vasilenko, V.; Amin, V. A.; Reuter, M. G.; Weiss, E. A. Model for Adsorption of Ligands to Colloidal Quantum Dots with Concentration-Dependent Surface Structure. *ACS Nano* **2012**, *6*, 557−565.
(40) Hu, R.; Yakovlev, D. R.; Liang, P.; Qiang, G.; Chen, C.; Jia, T.; Sun, Z.; Bayer, M.; Feng, D. Origin of Two Larmor Frequencies in the Coherent Spin Dynamics of Colloidal CdSe Quantum Dots Revealed by Controlled Charging. *J. Phys. Chem. Lett.* **2019**, *10*, 3681−3687.
(41) Feng, D.; Yakovlev, D. R.; Pavlov, V. V.; Rodina, A. V.; Shornikova, E. V.; Mund, J.; Bayer, M. Dynamic Evolution from Negative to Positive Photocharging in Colloidal CdS Quantum Dots. *Nano Lett.* **2017**, *17*, 2844−2851.

https://doi.org/10.1021/acs.jpclett.4c01543
J. Phys. Chem. Lett. 2024, 15, 7133−7140